Magnetostratigraphic Evidence for Post-Depositional Distortion of Osmium Isotopic Records in Pelagic Clay and Its Implications for Mineral Flux Estimates

Yoichi Usui (yoichi@jamstec.go.jp)
Japan Agency for Marine-Earth Science and Technology https://orcid.org/0000-0003-2365-2485
Toshitsugu Yamazaki
The University of Tokyo: Tokyo Daigaku

Express Letter

Keywords: Deep sea sediments, chronology, Eocene, Oligocene, diagenesis, bioturbation, eolian dust, rare-earth elements

Posted Date: September 22nd, 2020

DOI: https://doi.org/10.21203/rs.3.rs-78688/v1

Version of Record: A version of this preprint was published on January 4th, 2021. See the published version at https://doi.org/10.1186/s40623-020-01338-4.

Abstract

Chemical stratigraphy is useful for dating deep sea sediments which sometimes lack radiometric or biostratigraphic constraints. Oxic pelagic clay contains Fe-Mn oxyhydroxides that can retain seawater $^{187}Os/^{188}Os$ values, and its age can be estimated by fitting the isotopic ratios to the seawater $^{187}Os/^{188}Os$ curve. On the other hand, the stability of Fe-Mn oxyhydroxides is sensitive to redox change, and it is not clear whether the original $^{187}Os/^{188}Os$ values are always preserved in sediments. However, due to the lack of independent age constraints, the reliability of $^{187}Os/^{188}Os$ ages of pelagic clay have never been tested. Here we report inconsistency between magnetostratigraphic and $^{187}Os/^{188}Os$ ages in pelagic clay around Minamitorishima Island. In a ~ 5 m thick interval, previous studies correlated $^{187}Os/^{188}Os$ data to a brief (< 2 million years) isotopic excursion in the late Eocene. Paleomagnetic measurements revealed at least 12 polarity zones in the interval, indicating a > 3.3–7.4 million years duration. Quartz and feldspars content showed that while the paleomagnetic chronology gives reasonable eolian flux estimates, the $^{187}Os/^{188}Os$ chronology leads unrealistically high values. These results suggest that the low $^{187}Os/^{188}Os$ signal has diffused from an original thin layer to the current ~ 5 m interval, causing an underestimate of the deposition duration. The preservation of the polarity patterns indicates that a mechanical mixing such as bioturbation cannot be the main process for the diffusion, so diagenetic re-distribution of Fe-Mn oxyhydroxides and associated Os may be responsible. The paleomagnetic chronology presented here also demands reconsiderations of the timing, accumulation rate, and origins of the high content of rare-earth elements and yttrium in pelagic clay around Minamitorishima Island.

1. Introduction

Hydrogenous Os isotopic ratios are useful chronological markers for unfossiliferous pelagic clay, especially around the Eocene - Oligocene boundary (e.g., Peucker-Ehrenbrink and Ravizza 2012). Oxic pelagic clay contains Fe-Mn oxyhydroxides precipitated from seawater (e.g., Uramoto et al. 2019). These oxyhydroxides capture osmium in seawater (Koide et al. 1991) and record the $^{187}Os/^{188}Os$ at the time of deposition. In the late Eocene, seawater $^{187}Os/^{188}Os$ show a large excursion to unradiogenic (low $^{187}Os/^{188}Os$) values (Ravizza and Peucker-Ehrenbrink 2003). This excursion was identified not only in pelagic clay (Pegram and Turekian 1999) and ferromanganese crusts (Klemm et al. 2005; Nielsen et al. 2009), but also biogenic sediments with high resolution biostratigraphic and magnetostratigraphic age models (Ravizza and Peucker-Ehrenbrink 2003; Dalai et al. 2006). The age of the $^{187}Os/^{188}Os$ minima was estimated to be 34.5 ± 0.1 Ma (Dalai et al. 2006). It has also been proposed that dating of pelagic clay with ~ 0.1 million-year (Myr) resolution is possible by matching the shape of the excursion (Dalai et al. 2006; Nozaki et al. 2019; Ohta et al. 2020). However, the reliability of this method critically depends on the assumptions that Fe-Mn oxyhydroxides are hydrogenous and have been stable since deposition (e.g., Peucker-Ehrenbrink and Ravizza 2000).

Processes such as bioturbation and diagenesis can diffuse Fe-Mn oxyhydroxides either mechanically or chemically, so they can potentially distort the Os isotopic records. Bioturbation appears to be ubiquitous, even in the pelagic clay of oligotrophic oceans (e.g., Rutledge et al. 1995; Expedition 329 Scientists 2011). Detailed geochemical studies of sediments and Fe-Mn nodules in the northeast equatorial Pacific suggested that deep sea redox condition may have varied in response to surface productivity changes even if it is oxic at present (Mewes et al. 2014; Wegorzewski and Kuhn 2014). Diagenetic Fe-Mn micronodules were reported from surface clay in the western Pacific (Li et al. 2020). Abundant magnetite produced by magnetotactic bacteria were also found in oxic pelagic clay (Yamazaki and Shimono 2013; Shimono and Yamazaki 2016; Usui et al. 2017, 2019). These bacteria are thought to live near oxic/anoxic transition, indicating the presence of reducing microenvironment (Yamazaki and Shimono 2013).

Because pelagic clay generally has a slow sedimentation rate (< 1 m/Myr), post-depositional modifications would affect the reliability of $^{187}Os/^{188}Os$ stratigraphy. To date, however, no pelagic clay with $^{187}Os/^{188}Os$ data have been accompanied by independent age constraints with sufficient resolution to confirm the stability of the isotopic records. In this study, we report the magnetostratigraphy within the putative late Eocene $^{187}Os/^{188}Os$ excursion in pelagic clay around Minamitorishima Island. Flux estimates for eolian dust and fish debris are discussed to evaluate the different chronologies.

2. Materials

We studied pelagic clay recovered by a piston core MR14-E02 PC11 around Minamitorishima Island at 154°00.98' E, 22°59.02' N, and 5,647 m water depth. A $^{187}Os/^{188}Os$ excursion in this core was interpreted as the late Eocene excursion (Nozaki et al. 2019), as well as in a nearby core KR13-02 PC05 (Ohta et al., 2020). Geochemical and magnetic correlations confirmed that they are in the same stratigraphic position (Tanaka et al. 2020; Yamazaki et al. 2020).

In both cores, the $^{187}Os/^{188}Os$ excursions roughly coincide with the high concentrations (> 2000 ppm) of rare-earth elements and yttrium (REY), labeled as the 1st REY peak (Iijima et al. 2016; Tanaka et al. 2020). REY in pelagic clay are mainly carried by fish debris consisting of biogenic apatite (Kashiwabara et al. 2014, 2018; Yasukawa et al. 2016), especially in this region (Takaya et al. 2018; Yasukawa et al. 2019). From these observations, Ohta et al. (2020) proposed that fish production increased significantly at ~ 34.4 Ma in response to the expansion of the Antarctic ice sheet (Katz et al. 2008).

3. Methods

3.1. Paleomagnetism and rock magnetism

Progressive AF demagnetizations of natural remanence were conducted using a cryogenic magnetometer 2G Enterprises 760 at the Center for Advanced Marine Core Research (CMCR), Kochi University. The results were analyzed by principal component analysis to isolate characteristic remanence (Kirschvink, 1980). Chronostratigraphy was estimated by comparing the polarity patterns with the geomagnetic polarity time scale (GPTS) in Geological Time Scale 2012 (Ogg 2012).

Magnetic properties of the samples were examined to help paleomagnetic interpretation. We measured the ratio of anhysteretic remanence (ARM) susceptibility (κ_{ARM}) to saturation isothermal remanence (SIRM) and S ratios. In the Minamitorishima region, κ_{ARM}/SIRM reflects the abundance of biogenic magnetite relative to terrigenous magnetic minerals (Usui et al., 2017; Usui et al., 2019; Yamazaki et al., 2020). After paleomagnetic measurements, ARMs were imparted with a 0.1 mT DC field and 80 mT peak AF field using the cryogenic magnetometer at CMCR. IRMs were imparted with 2.5 T field using a pulse magnetizer Magnetic Measurements model MMPM-10 at Atmosphere and Ocean Research Institute, the University of Tokyo. S ratios measures the relative abundance of minerals with contrasting coercivity. SIRM measurements were followed by IRMs imparted by back fields of -0.1 and − 0.3 T. S ratios ($S_{-0.1}$ and $S_{-0.3}$) were calculated following the definition of Bloemendal et al. (1988). In pelagic sediments, $S_{-0.1}$ and $S_{-0.3}$ often reflect the relative abundance of biogenic magnetite to abiotic magnetic minerals, and ferromagnetic minerals to antiferromagnetic minerals (e.g., hematite), respectively.

3.2. Quartz and feldspar content

To quantify eolian dust content, we separated quartz and feldspars using the sodium pyrosulfate ($Na_2S_2O_7$) fusion method (Syers et al. 1968; Clayton et al. 1972; Blatt et al. 1982; Stevens 1991; Usui et al. 2018). Dry samples of ~ 1 g were first treated with citrate-sodium dithionite solution buffered with sodium bicarbonate to remove poorly crystalline Fe–Mn oxyhydroxides (Rea and Janecek 1981). The residues were washed with purified water, freeze-dried, weighed, and treated with acetic acid overnight, which has been assumed to remove carbonate and apatite. The residues were washed, freeze-dried, weighed, and fused with $Na_2S_2O_7$ at 460 °C. The fusions were treated with 3N HCl and washed with purified water. Then, the residues were heated to 50 °C in 1M NaOH overnight.

4. Results

4.1. Rock magnetism

Rock magnetic properties showed smooth variations (Fig. 1). κ_{ARM}/SIRM were ~ 1 mm/A down to ~ 6 m. They increased to > 2.0 mm/A below ~ 7 m into the 1st REY peak, indicating dominance of biogenic magnetite over terrigenous magnetic minerals. These behaviors are consistent with a nearby cores (Usui et al. 2017; Yamazaki et al. 2020). S ratios were high, indicating limited contribution from antiferromagnetic minerals. $S_{-0.1}$ were close to 1 between ~ 6–12 m (Fig. 1b), indicating dominance of low coercivity minerals such as biogenic magnetite. $S_{-0.3}$ were slightly lower below ~ 12 m (chemostratigraphic Unit III of Tanaka et al., 2020), suggesting an increase in antiferromagnetic minerals such as hematite.

4.2. Paleomagnetism

Clear polarity patterns were obtained at limited intervals (Fig. 1c and d). Top ~ 8 m was characterized by stable declination with apparently normal polarity (positive inclination; Fig. 1d). Considering the proposed chronology (~ 34 Ma at ~ 7 m; Nozaki et al., 2019), we interpreted this normal polarity zone as reflecting viscous overprint and cancellation of dual polarity signal due to slow sedimentation. This interpretation is partly supported by the presence of large normal polarity overprints in samples with characteristic remanence with negative inclinations (Fig. 1g). Below ~ 8 m, the core showed 12 polarity zones with comparable lengths.

4.3. Quartz and feldspars content

The CBD treatment reduced the sample weight by 10–20% (Fig. 2). This can be considered as approximated weight fractions of Fe-Mn oxyhydroxides. The weight change was ~ 10% at the top, gradually increased with depth to ~ 15–20% towards ~ 6 m.

Acetic acid treatment further reduced the weight; the change was largest in ~ 7–12 m where REY concentrations were high. This is consistent with the interpretation that fish debris carry REY (Iijima et al. 2016; Ohta et al. 2020). However, the change was at most ~ 5% of the original weight. On the other hand, there is a strong linear relationship between P_2O_5 and REY content in sediments around Minamitorishima Island (Iijima et al. 2016; Takaya et al. 2018), suggesting fraction of fish debris is nearly proportional to REY content. Using data from KR13-02 PC05 (Ohta et al. 2020), we can estimate that MR14-E02 PC11 clay (REY content up to 4000 ppm) contains up to ~ 20 wt.% of fish debris. It is thus likely that acetic acid treatment does not remove biogenic apatite effectively.

$Na_2S_2O_7$ fusion further reduced the sample weight to ~ 15–30 wt.% of the original weight (Fig. 2). We consider these weights as the quartz and feldspars content. The highest content was from the top of the core. Below 7 m, it was ~ 15 wt.%. Note that these numbers are affected by Fe-Mn oxyhydroxides and fish debris content; given ~ 15 wt.% of Fe-Mn oxyhydroxides and up to ~ 20 wt.% of fish debris below 7 m, the weight fraction of quartz and feldspar relative to total silicate may be ~ 20–30 wt.% throughout the core.

5. Discussion

Paleomagnetic data show that there are at least 12 polarity zones in 8–12 m (Fig. 1). $^{187}Os/^{188}Os$ were as low as 0.3 in 7–12 m (Fig. 3), and previous interpretations correlated them to the late Eocene excursion (Nozaki et al., 2019; Fig. 3). However, this interpretation would put 7–12 m into a single chron of C13r. Rock magnetic properties change smoothly in this interval (Fig. 1), so these polarity zones are likely to reflect the geomagnetic reversals rather than short scale variations in overprint.

Because there are only ichthyoliths stratigraphy constraints suggesting late Eocene – early Oligocene ages for the corresponding 1st REY peak in KR13-02 PC05 (Ohta et al., 2020), we cannot correlate the observed polarity zones with GPTS uniquely. Nonetheless, based on the ichthyoliths data and the low $^{187}Os/^{188}Os$, we infer that the late Eocene $^{187}Os/^{188}Os$ excursion (~ 34.5 Ma) is somewhere in 7–12 m. With this inference, we can list possible correlations with GPTS (Table 1). The deepest polarity transition (11.96 m), which coincide with the beginning of the 1st REY peak, would be between 34.999 to 38.615 Ma, and the shallowest polarity transition (8.67 m), which is deeper than the end of the 1st REY peak (7 m), would be between 28.087 to 35.294 Ma. All of these magnetostratigraphic correlations indicate that the deposition of the 1st REY peak took much longer (3.3–7.4 Myr) than the $^{187}Os/^{188}Os$ ages (< 1 Myr; Nozaki et al., 2019; Ohta et al., 2020).

Inconsistency between the magnetostratigraphy and $^{187}Os/^{188}Os$ ages can be compared in terms of the eolian flux. The chemical digestion results (Fig. 2) show that quartz and feldspars account for ~ 10–20 wt.% of the dry sediment of the 1st REY peak. $^{187}Os/^{188}Os$ suggest the sedimentation rate of ~ 3.3 m/Myr for the 1st REY peak of MR14-E02 PC12 (Nozaki et al., 2019). Using a typical dry bulk density of 500 kg/m^3 (Ohta et al., 2020), these numbers are converted to a quartz and feldspars flux of ~ 165–330 kg/m^2/Myr. Typically, quartz and feldspars account for 10–20 wt.% of eolian dust (Blank et al. 1985; Leinen et al. 1994; Usui et al. 2018), which is broadly consistent with our estimate of ~ 20–30 wt.% of the silicate. These numbers indicate > 500 kg/m^2/Myr of eolian flux. This is comparable to the current flux to the Pacific at ~ 16 ºN (Rea, 1994), where Minamitorishima Island was at ~ 35 Ma. However, multiple records from the North Pacific indicated that the eolian flux has increased by more than tenfold since 25 Ma (e.g., Zhang et al. 2016). Only a few estimates exist for flux before 30 Ma, but it may be even smaller between 35–45 Ma (Janecek and Rea 1983; Janecek 1985). Thus, the flux estimates based on the $^{187}Os/^{188}Os$ seem too large. In contrast, magnetostratigraphy suggests sedimentation rates of 0.44–0.99 m/Myr in the 1st REY peak (Table 1). They are converted to eolian flux estimates of ~ 70–500 kg/m^2/Myr. The lower end of the range is consistent with the evolution of the eolian flux in the North Pacific. Therefore, we argue that the $^{187}Os/^{188}Os$ ages overestimate the sedimentation rate of the 1st REY peak. We further consider that GPTS correlations which give slower sedimentation rates (< 0.5 m/Myr) are more plausible, implying that the deposition of 1st REY took more than 6.5 Myr and completed more recently than 31 Ma (Table 1).

The proposed revision of the chronology for the 1st REY peak affects the estimates of fish debris accumulation rates and the origin of the REY peaks. On the basis of the $^{187}Os/^{188}Os$ ages, Ohta et al. (2020) estimated high fish debris accumulation rates of > 300 kg/m^2/Myr for the 1st REY peak in KR13-02 PC05. Our paleomagnetic data indicate that the deposition of the 1st REY peak may have taken 10–30 times longer; the eolian flux estimates prefer the larger end of the range. Therefore, we suggest that the maximum fish debris accumulation rate in the 1st REY peak was on the order of 10 kg/m^2/Myr. Indeed, assuming a fish debris content of 20 wt.%, the maximum fish debris accumulation rate for MR14-E02 PC11 can be estimated as 44–99 kg/m^2/Myr. The fact that the REY content shows sharp maxima even within the 1st REY peak indicates significant temporal variation of the fish debris accumulation. Cenozoic fish debris accumulation rate in the central North Pacific can be estimated using data from the core LL44-GPC3 (Kyte et al. 1993). Assuming that P_2O_5 is exclusively in fish debris at ~ 30 wt.% (Kon et al. 2014; Takaya et al. 2018), the estimated rate was mostly below 10 kg/m^2/Myr except for a peak at ~ 66 Ma and another, smaller peak at ~ 58 Ma (see Additional file 1). Thus, the formation of the 1st REY peak around Minamitorishima Island still requires an explanation.

Ohta et al. (2020) suggested that the enhanced fish debris accumulation is related to the bottom water upwelling during the brief ice volume expansion at ~ 34.15 Ma (Katz et al., 2008). While upwelling is still a viable hypothesis, the paleomagnetic chronology indicates that the 1st REY peak reflects longer-term changes in ocean circulations. The present paleomagnetic chronology cannot place unique ages (Table 1); a better chronology is needed to test the connections to specific paleoenvironmental events for the beginning and end of the 1st REY peak.

$^{187}Os/^{188}Os$ in the 1st REY peak are all close to the minimum values reported for the late Eocene excursion (Fig. 3). The magnetostratigraphy requires homogenization of $^{187}Os/^{188}Os$. Complete mechanical mixing by processes such as bioturbation over ~ 5 m interval is unlikely, and they would also destroy the polarity records. So, we suspect chemical remobilization of Fe-Mn oxyhydroxides as a cause of the homogeneous $^{187}Os/^{188}Os$. The 1st REY peak represents enhanced flux of fish debris, which may have brought oxic-anoxic transition zone to shallow depths, promoting diagenetic movement of Mn (Mewes et al. 2014; Wegorzewski and Kuhn 2014).

A simple averaging of the seawater $^{187}Os/^{188}Os$ curve does not yield long-term lows as observed in the core (Fig. 3). We note three factors that help to resolve this inconsistency. First, Os influx to sediment may be variable, so homogenization involves taking weighted averages. If the original Os deposition was sufficiently larger during the isotopic excursion than other period, then the $^{187}Os/^{188}Os$ after homogenization would be low, and Os content would be high. This is qualitatively consistent with the elevated Os content in the 1st REY peak of KR13-02 PC05 (Ohta et al., 2020); however, the Os content of MR14-E02 PC11 does not show a similar pattern (Nozaki et al., 2019), so the contribution of this factor may be limited. Second, $^{187}Os/^{188}Os$ may not be globally uniform, so the comparison of the absolute values may not be appropriate (e.g., Peucker-Ehrenbrink and Ravizza 2012). Finally, the $^{187}Os/^{188}Os$ of pelagic sediments may be contaminated by unradiogenic extraterrestrial components to yield lower values (e.g., Peucker-Ehrenbrink and Ravizza 2000). The $^{187}Os/^{188}Os$ in the Minamitorishima samples were analyzed using the Carius tube methods with reverse aqua regia (Shirey and Walker 1995). Some argued that more diluted leaching solution (0.15% H_2O_2) should be used to minimize the effect of extraterrestrial components (Turekian and Pegram 1997). These factors may affect the $^{187}Os/^{188}Os$ dating outside the 1st REY peak as well.

6. Conclusion

Magnetostratigraphy of MR14-E02 PC11 indicates 3.3–7.4 Myr duration for the deposition of a layer where $^{187}Os/^{188}Os$ was previously correlated to a < 2 Myr excursion. Eolian flux estimates based on the direct measurements of quartz and feldspar content support that a duration longer than 6.5 Myr is plausible. The inconsistency may be resulted from diagenetic redistribution of Fe-Mn oxyhydroxides and associated Os under high biogenic flux. The revised chronology indicates that the fish debris accumulation rate in the interval was an order of magnitude lower than the previous estimates; nonetheless, it may be still

significantly higher than other area or time. The elevated fish debris flux is likely to be associated with long term oceanographic changes rather than a single event. Our results indicate that high resolution dating of pelagic clay using $^{187}Os/^{188}Os$ should be conducted with care.

7. Abbreviations

Myr: million-year

REY: Rare-earth elements and yttrium

ARM: anhysteretic remanence

SIRM: saturation isothermal remanence

IRM: isothermal remanence

CMCR: The Center for Advanced Marine Core Research

GPTS: Geomagnetic polarity time scale

8. Declarations

Ethics approval and consent to participate

Not applicable

Consent for publication

Not applicable

Availability of data and materials

All data produced in this work are available in Zenodo repository (doi: 10.5281/zenodo.4023918).

Competing interests

The authors declare that they have no competing interests.

Funding

This work was supported by JSPS KAKENHI grant numbers JP17H01361and JP17H04855.

Authors' contributions

YU and TY contributed conceptualization. YU conducted chemical digestion analyses, wrote the original draft. TY conducted magnetic analyses, reviewed and edited the draft.

Acknowledgements

This study was performed under the cooperative research program of CMCR, Kochi University 15A022 and 15B019. The authors acknowledge Drs. Tatsuo Nozaki and Junichiro Ohta for sharing the compilation of seawater $^{187}Os/^{188}Os$ and stimulating discussion, Erika Tanaka and Kazuhide Mimura for information on the chemical composition of LL44-GPC3. YU thanks Aguri Irisawa for the help in the laboratory.

9. References

1. Blank M, Leinen M, Prospero JM (1985) Major Asian aeolian inputs indicated by the mineralogy of aerosols and sediments in the western North Pacific. Nature 314:84–86. https://doi.org/10.1038/314084a0
2. Blatt H, Jones RL, Charles RG (1982) Separation of quartz and feldspars from mudrocks. J Sediment Petrol 52:660–662. https://doi.org/10.2110/jsr.52.660
3. Bloemendal J, Lamb B, King J (1988) Paleoenvironmental implications of rock-magnetic properties of Late Quaternary sediment cores from the eastern equatorial Atlantic. Paleoceanography 3:61–87. https://doi.org/10.1029/PA003i001p00061
4. Clayton RN, Rex RW, Syers JK, Jackson ML (1972) Oxygen isotope abundunce in quartz from Pacific pelagic sediments. J Geophys Res 77:3907–3915
5. Dalai TK, Ravizza GE, Peucker-Ehrenbrink B (2006) The Late Eocene 187Os/188Os excursion: Chemostratigraphy, cosmic dust flux and the Early Oligocene glaciation. Earth Planet Sci Lett 241:477–492. https://doi.org/10.1016/j.epsl.2005.11.035
6. Expedition 329 Scientists (2011) Site U1365. In: D'Hondt S, Inagaki F, Zarikian CA, Scientists E 329 Proc. IODP, 329. Integrated Ocean Drilling Program Management International, Inc., Tokyo

7. Hatakeyama T (2018) Online plotting applications for paleomagnetic and rock magnetic data. Earth, Planets Sp 70:139. https://doi.org/10.1186/s40623-018-0906-5
8. Iijima K, Yasukawa K, Fujinaga K, Nakamura K, Machida S, Takaya Y, Ohta J, Haraguchi S, Nishio Y, Usui Y, Nozaki T, Yamazaki T, Ichiyama Y, Ijiri A, Inagaki F, Machiyama H, Suzuki K, Kato Y (2016) Discovery of extremely REY-rich mud in the western North Pacific Ocean. Geochem J 50:557–573. https://doi.org/10.2343/geochemj.2.0431
9. Janecek TR (1985) 26. Eolian sedimentation in the northwest Pacific Ocean: A preliminary examination of the data from Deep Sea Drilling Project Sites 576 and 578. In: Ross Heath G, Burckle LH, et al. (eds) Initial Reports of the Deep Sea Drilling Project, 86. U.S. Government Printing Office, Washington, pp 589–603
10. Janecek TR, Rea DK (1983) Eolian deposition in the northeast Pacific Ocean: Cenozoic history of atmospheric circulation. GSA Bull 94:730–738. https://doi.org/10.1130/0016-7606(1983)94<730:editnp>2.0.co;2
11. Kashiwabara T, Toda R, Fujinaga K, Honma T, Takahashi Y, Kato Y (2014) Determination of Host Phase of Lanthanum in Deep-sea REY-rich Mud by XAFS and μ-XRF Using High-energy Synchrotron Radiation. Chem Lett 43:199–200. https://doi.org/10.1246/cl.130853
12. Kashiwabara T, Toda R, Nakamura K, Yasukawa K, Fujinaga K, Kubo S, Nozaki T, Takahashi Y, Suzuki K, Kato Y (2018) Synchrotron X-ray spectroscopic perspective on the formation mechanism of REY-rich muds in the Pacific Ocean. Geochim Cosmochim Acta 240:274–292. https://doi.org/10.1016/J.GCA.2018.08.013
13. Katz ME, Miller KG, Wright JD, Wade BS, Browning J V., Cramer BS, Rosenthal Y (2008) Stepwise transition from the Eocene greenhouse to the Oligocene icehouse. Nat Geosci 1:329–334. https://doi.org/10.1038/ngeo179
14. Klemm V, Levasseur S, Frank M, Hein JR, Halliday AN (2005) Osmium isotope stratigraphy of a marine ferromanganese crust. Earth Planet Sci Lett 238:42–48. https://doi.org/10.1016/j.epsl.2005.07.016
15. Koide M, Goldberg ED, Niemeyer S, Gerlach D, Hodge V, Bertine KK, Padova A (1991) Osmium in marine sediments. Geochim Cosmochim Acta 55:1641–1648. https://doi.org/10.1016/0016-7037(91)90135-R
16. Kon Y, Hoshino M, Sanematsu K, Morita S, Tsunematsu M, Okamoto N, Yano N, Tanaka M, Takagi T (2014) Geochemical characteristics of apatite in heavy REE-rich Deep-Sea Mud from Minami-Torishima Area, Southeastern Japan. Resour Geol 64:47–57. https://doi.org/10.1111/rge.12026
17. Kyte FT, Leinen M, Ross Heath G, Zhou L (1993) Cenozoic sedimentation history of the central North Pacific: Inferences from the elemental geochemistry of core LL44-GPC3. Geochim Cosmochim Acta 57:1719–1740. https://doi.org/10.1016/0016-7037(93)90109-A
18. Leinen M, Prospero JM, Arnold E, Blank M (1994) Mineralogy of aeolian dust reaching the North Pacific Ocean: 1. Sampling and analysis. J Geophys Res 99:21017. https://doi.org/10.1029/94JD01735
19. Li D, Fu Y, Liu Q, Reinfelder JR, Hollings P, Sun X, Tan C, Dong Y, Ma W (2020) High-resolution LA-ICP-MS mapping of deep-sea polymetallic micronodules and its implications on element mobility. Gondwana Res 81:461–474. https://doi.org/10.1016/j.gr.2019.12.009
20. Mewes K, Mogollón JM, Picard A, Rühlemann C, Kuhn T, Nöthen K, Kasten S (2014) Impact of depositional and biogeochemical processes on small scale variations in nodule abundance in the Clarion-Clipperton Fracture Zone. Deep Sea Res Part I Oceanogr Res Pap 91:125–141. https://doi.org/10.1016/j.dsr.2014.06.001
21. Nielsen SG, Mar-Gerrison S, Gannoun A, LaRowe D, Klemm V, Halliday AN, Burton KW, Hein JR (2009) Thallium isotope evidence for a permanent increase in marine organic carbon export in the early Eocene. Earth Planet Sci Lett 278:297–307. https://doi.org/10.1016/j.epsl.2008.12.010
22. Nozaki T, Ohta J, Noguchi T, Sato H, Ishikawa A, Takaya Y, Kimura JI, Chang Q, Shimada K, Ishibashi J ichiro, Yasukawa K, Kimoto K, Iijima K, Kato Y (2019) A Miocene impact ejecta layer in the pelagic Pacific Ocean. Sci Rep 9:1–9. https://doi.org/10.1038/s41598-019-52709-1
23. Ogg JG (2012) Geomagnetic Polarity Time Scale. In: Gradstein FM, Ogg JG, Schmitz MM, Ogg GM (eds) The Geologic Time Scale 2012. Elsevier B.V., pp 85–113
24. Ohta J, Yasukawa K, Nozaki T, Takaya Y, Mimura K, Fujinaga K, Nakamura K, Usui Y, Kimura JI, Chang Q, Kato Y (2020) Fish proliferation and rare-earth deposition by topographically induced upwelling at the late Eocene cooling event. Sci Rep 10:1–11. https://doi.org/10.1038/s41598-020-66835-8
25. Pegram WJ, Turekian KK (1999) The osmium isotopic composition change of Cenozoic sea water as inferred from a deep-sea core corrected for meteoritic contributions. Geochim Cosmochim Acta 63:4053–4058. https://doi.org/10.1016/s0016-7037(99)00308-7
26. Peucker-Ehrenbrink B, Ravizza G (2000) The marine osmium isotope record. Terra Nova 12:205–219. https://doi.org/10.1046/j.1365-3121.2000.00295.x
27. Peucker-Ehrenbrink B, Ravizza GE (2012) Osmium Isotope Stratigraphy. In: Gradstein FM, Ogg JG, Schmitz MD, Ogg, Gabi M (eds) The Geologic Time Scale 2012. Elsevier B.V., pp 145–166
28. Ravizza G, Peucker-Ehrenbrink B (2003) The marine 187Os/188Os record of the Eocene-Oligocene transition: The interplay of weathering and glaciation. Earth Planet Sci Lett 210:151–165. https://doi.org/10.1016/S0012-821X(03)00137-7
29. Rea DK, Janecek TR (1981) Late cretaceous history of eolian deposition in the mid-pacific mountains, central North Pacific Ocean. Palaeogeogr Palaeoclimatol Palaeoecol 36:55–67. https://doi.org/10.1016/0031-0182(81)90048-1
30. Rutledge AK, Roberts JA, Orsi TH, Bryant WR, Kotilainen AT (1995) 35. Geotechnical properties and consolidation characteristics of north Pacific sediments, Sites 881, 883, and 885/886. In: Rea DK, Basov IA, Scholl IA, Allan JF, et al. (eds) Proceedings of the Ocean Drilling Program, 145 Scientific Results. Ocean Drilling Program, College Station, pp 525–546
31. Shimono T, Yamazaki T (2016) Environmental rock-magnetism of Cenozoic red clay in the South Pacific Gyre. Geochemistry, Geophys Geosystems 17:1296–1311. https://doi.org/10.1002/2015GC006062
32. Shirey SB, Walker RJ (1995) Carius Tube Digestion for Low-Blank Rhenium-Osmium Analysis. Anal Chem 67:2136–2141. https://doi.org/10.1021/ac00109a036

33. Stevens RL (1991) Grain-size distribution of quartz and feldspar extracts and implications for flocculation processes. Geo-Marine Lett 11:162–165. https://doi.org/10.1007/BF02431004
34. Syers JK, Chapman SL, Jackson ML, Rex RW, Clayton RN (1968) Quartz isolation from rocks, sediments and soils for determination of oxygen isotopes composition. Geochim Cosmochim Acta 32:1022–1025. https://doi.org/10.1016/0016-7037(68)90067-7
35. Takaya Y, Yasukawa K, Kawasaki T, Fujinaga K, Ohta J, Usui Y, Nakamura K, Kimura J-I, Chang Q, Hamada M, Dodbiba G, Nozaki T, Iijima K, Morisawa T, Kuwahara T, Ishida Y, Ichimura T, Kitazume M, Fujita T, Kato Y (2018) The tremendous potential of deep-sea mud as a source of rare-earth elements. Sci Rep 8:5763. https://doi.org/10.1038/s41598-018-23948-5
36. Tanaka E, Nakamura K, Yasukawa K, Mimura K, Fujinaga K, Iijima K, Nozaki T, Kato Y (2020) Chemostratigraphy of deep-sea sediments in the western North Pacific Ocean: Implications for genesis of mud highly enriched in rare-earth elements and yttrium. Ore Geol Rev 119:103392. https://doi.org/10.1016/j.oregeorev.2020.103392
37. Turekian KK, Pegram WJ (1997) Os Isotope Record in a Cenozoic Deep-Sea Core: Its Relation to Global Tectonics and Climate. In: Ruddiman W (ed) Tectonic Uplift and Climate Change. Springer, Boston, pp 383–397
38. Uramoto G-I, Morono Y, Tomioka N, Wakaki S, Nakada R, Wagai R, Uesugi K, Takeuchi A, Hoshino M, Suzuki Y, Shiraishi F, Mitsunobu S, Suga H, Takeichi Y, Takahashi Y, Inagaki F (2019) Significant contribution of subseafloor microparticles to the global manganese budget. Nat Commun 10:400. https://doi.org/10.1038/s41467-019-08347-2
39. Usui Y, Shimono T, Yamazaki T (2018) Rock magnetism of quartz and feldspars chemically separated from pelagic red clay: a new approach to provenance study. Earth, Planets Sp 70:153. https://doi.org/10.1186/s40623-018-0918-1
40. Usui Y, Yamazaki T, Oka T, Kumagai Y (2019) Inverse Magnetic Susceptibility Fabrics in Pelagic Sediment: Implications for Magnetofossil Abundance and Alignment. J Geophys Res Solid Earth. https://doi.org/10.1029/2019JB018128
41. Usui Y, Yamazaki T, Saitoh M (2017) Changing Abundance of Magnetofossil Morphologies in Pelagic Red Clay Around Minamitorishima, Western North Pacific. Geochemistry, Geophys Geosystems 18:4558–4572. https://doi.org/10.1002/2017GC007127
42. Wegorzewski A V., Kuhn T (2014) The influence of suboxic diagenesis on the formation of manganese nodules in the Clarion Clipperton nodule belt of the Pacific Ocean. Mar Geol 357:123–138. https://doi.org/10.1016/j.margeo.2014.07.004
43. Yamazaki T, Fu W, Shimono T, Usui Y (2020) Unmixing biogenic and terrigenous magnetic mineral components in red clay of the Pacific Ocean using principal component analyses of first-order reversal curve diagrams and paleoenvironmental implications. Earth, Planets Sp 72:120. https://doi.org/10.1186/s40623-020-01248-5
44. Yamazaki T, Shimono T (2013) Abundant bacterial magnetite occurrence in oxic red clay. Geology 41:1191–1194. https://doi.org/10.1130/G34782.1
45. Yasukawa K, Nakamura K, Fujinaga K, Iwamori H, Kato Y (2016) Tracking the spatiotemporal variations of statistically independent components involving enrichment of rare-earth elements in deep-sea sediments. Sci Rep 6:1–12. https://doi.org/10.1038/srep29603
46. Yasukawa K, Ohta J, Miyazaki T, Vaglarov BS, Chang Q, Ueki K, Toyama C, Kimura JI, Tanaka E, Nakamura K, Fujinaga K, Iijima K, Iwamori H, Kato Y (2019) Statistic and Isotopic Characterization of Deep-Sea Sediments in the Western North Pacific Ocean: Implications for Genesis of the Sediment Extremely Enriched in Rare Earth Elements. Geochemistry, Geophys Geosystems 20:3402–3430. https://doi.org/10.1029/2019GC008214
47. Zhang W, Chen J, Ji J, Li G (2016) Evolving flux of Asian dust in the North Pacific Ocean since the late Oligocene. Aeolian Res 23:11–20. https://doi.org/10.1016/J.AEOLIA.2016.09.004

10. Table

Table 1
GPTS correlation models.

	Polarity transition ages (Ma)												
correlation #	8.67 m	8.86 m	9.17 m	9.62 m	10.03 m	10.39 m	10.73 m	11.01 m	11.24 m	11.56 m	11.88 m	11.96 m	LSR (m/Myr
1	28.087	28.141	28.278	29.183	29.477	29.527	29.97	30.591	31.034	33.157	33.705	34.999	0.48
2	28.278	29.183	29.477	29.527	29.97	30.591	31.034	33.157	33.705	34.999	35.294	35.706	0.44
3	29.477	29.527	29.97	30.591	31.034	33.157	33.705	34.999	35.294	35.706	35.892	36.051	0.50
4	29.97	30.591	31.034	33.157	33.705	34.999	35.294	35.706	35.892	36.051	36.7	36.969	0.47
5	31.034	33.157	33.705	34.999	35.294	35.706	35.892	36.051	36.7	36.969	37.753	37.872	0.48
6	33.705	34.999	35.294	35.706	35.892	36.051	36.7	36.969	37.753	37.872	38.093	38.159	0.74
7	35.294	35.706	35.892	36.051	36.7	36.969	37.753	37.872	38.093	38.159	38.333	38.615	0.99

Numerical ages are based on Ogg (2012). LSR: linear sedimentation rate for 11.96–8.67 m.

Figures

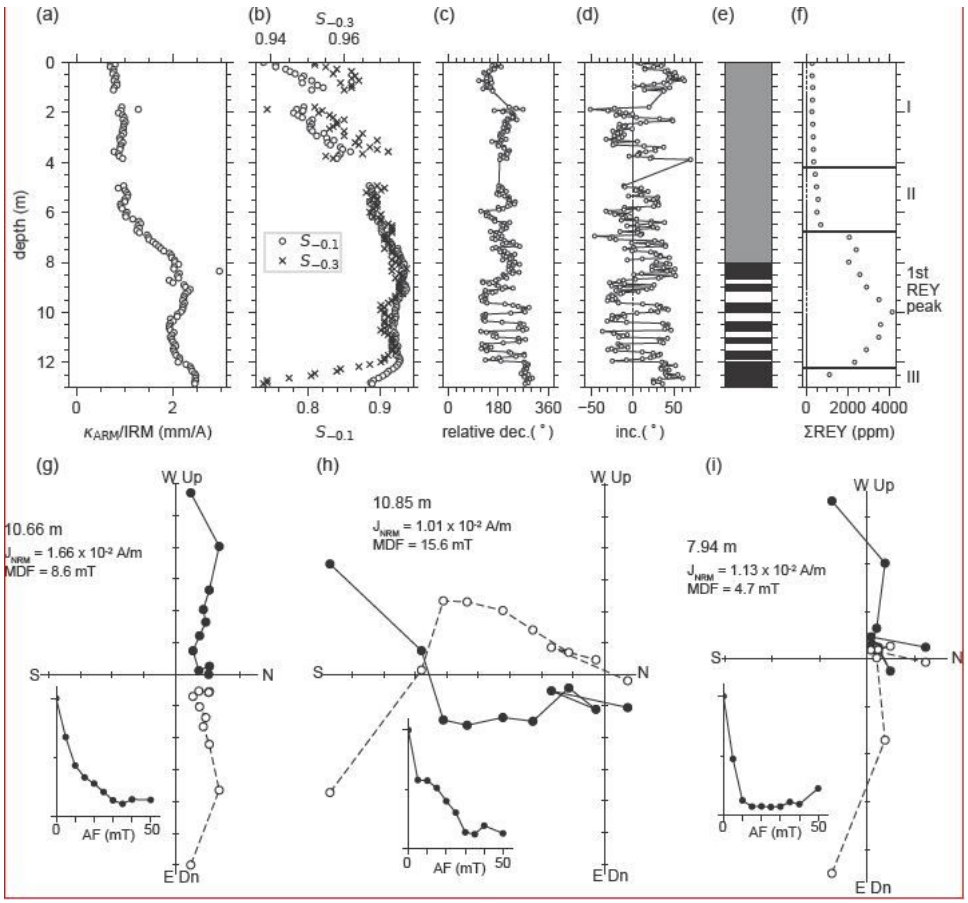

Figure 1

Depth variations of rock magnetic and paleomagnetic results. (a) κARM/SIRM. (b) S-ratios. Open circles represent S-0.1, and crosses represent S-0.3, (c) Relative declination. The core was not azimuthally oriented with respect to the geographic coordinates. (d) Inclination. (e) Interpreted polarity. Black represents normal polarity, white represents reversed polarity, and gray represents an interval of uncertain polarity (see text for discussion). (f) Variation of total REY content (Iijima et al., 2016). On the right are chemostratigraphic Units of Tanaka et al. (2020). (g-i) Representative orthogonal vector plots for samples with (g) normal polarity, (h) reversed polarity, and (i) normal polarity that was interpreted as dominantly overprinted (see text for discussion). Solid circles show the horizontal projection, and open circles show the vertical projection. Insets show decay of remanence intensity. Plot (g) - (i) were created by MagePlot/P (ver. 1.1; Hatakeyama 2018).

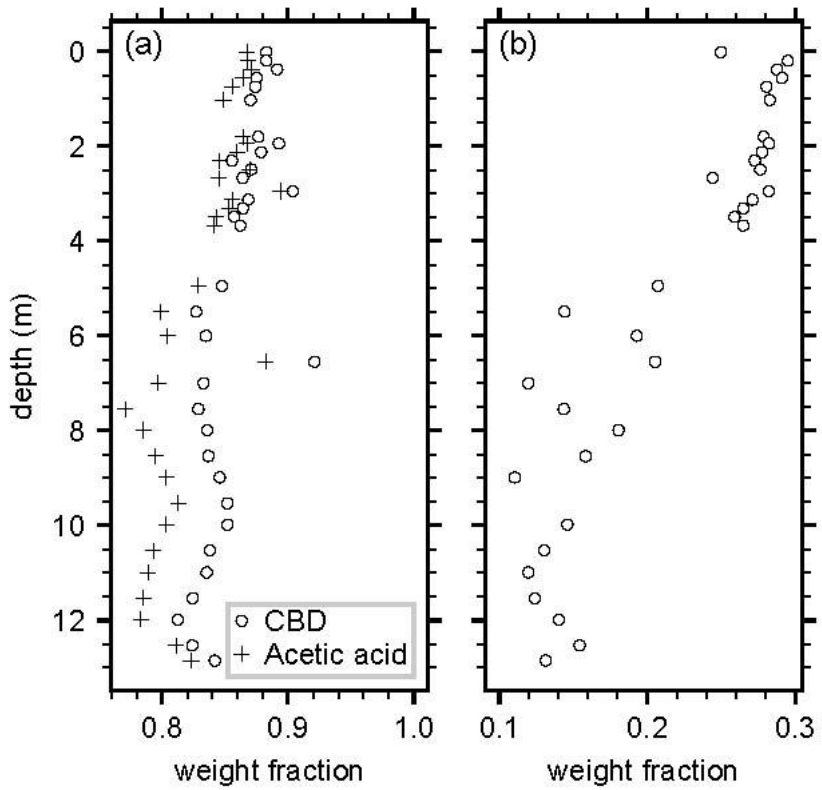

Figure 2

Chemical digestion results. (a) Weight fraction of residue after CBD treatment (open circles) and subsequent acetic acid treatment (crosses). (b) Weight fraction of residue after sodium pyrosulfate fusion.

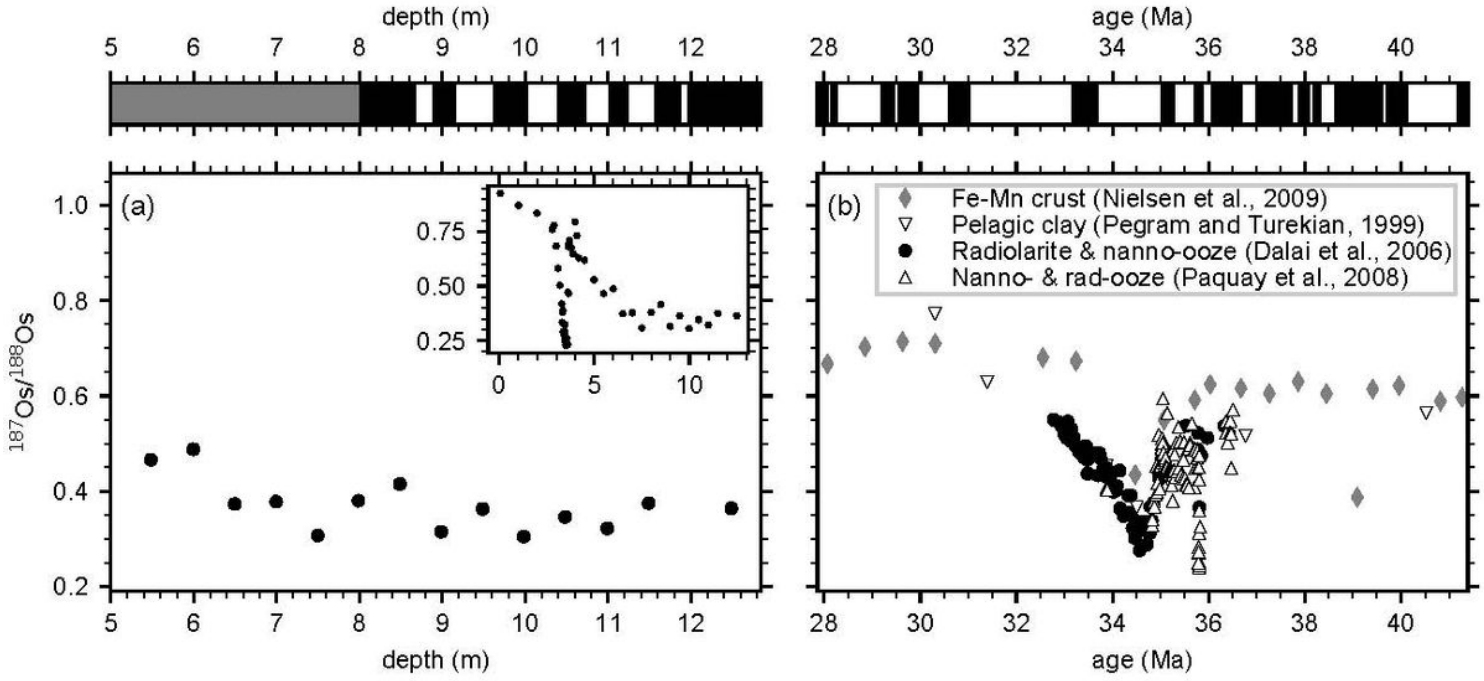

Figure 3

Comparisons of magnetostratigraphy and 187Os/188Os records. (a) Depth variation of 187Os/188Os (Nozaki et al., 2019) together with inferred polarity zones of MR14-E02 PC11 for 5-12 m (Figure 1). The inset is the 187Os/188Os for the entire core. A negative excursion at ~3.5 m was interpreted as a Miocene impact event (Nozaki et al., 2019). (b) Seawater 187Os/188Os data for 28-41 Ma together with the geomagnetic polarity (Ogg, 2012). The 187Os/188Os data are from ferromanganese crust (gray diamonds; Nielsen et al., 2011), pelagic clay (open inverted triangles; Pegram and Turekian, 1999), radiolarite and nannofossil ooze (filled circles; Dalai et al., 2006), and nannofossil and radiolarian ooze (Paquay et al., 2008). The chronology of ferromanganese crust was

based on the 187Os/188Os correlation to ~11-12 Ma, ~34.4 Ma, and ~55.5 Ma and linear interpolation between them with some adjustments. The chronology of pelagic clay is based on constant a Co flux model which may have 5-10 Myr offset in this interval (Kyte et al., 1993).

Supplementary Files

This is a list of supplementary files associated with this preprint. Click to download.

- graphicalabstract.jpg
- additionalfile1.xlsx